Symmetric and asymmetric solitons in linearly coupled Bragg gratings

William C. K. Mak,[1] Boris A. Malomed,[2,1] and Pak L. Chu[1]
[1]*Optoelectronic Research Centre, Department of Electronic Engineering, City University of Hong Kong*
[2]*Department of Interdisciplinary Studies, Faculty of Engineering, Tel Aviv University, Tel Aviv 69978, Israel*
(Received 8 August 2003; revised manuscript received 24 February 2004; published 14 June 2004)

We demonstrate that a symmetric system of two linearly coupled waveguides, with Kerr nonlinearity and resonant grating in both of them, gives rise to a family of symmetric and antisymmetric solitons in an exact analytical form, a part of which exists outside of the bandgap in the system's spectrum, i.e., they may be regarded as embedded solitons (ES's, i.e., the ones partly overlapping with the continuous spectrum). Parameters of the family are the soliton's amplitude and velocity. Asymmetric ES's, unlike the regular (nonembedded) gap solitons (GS's), do not exist in the system. Moreover, ES's exist even in the case when the system's spectrum contains no bandgap. The main issue is the stability of the solitons. We demonstrate that some symmetric ES's are stable, while all the antisymmetric solitons are unstable; an explanation is given to the latter property, based on the consideration of the system's Hamiltonian. We produce a full stability diagram, which comprises both embedded and regular solitons, quiescent and moving. A stability region for ES's is found around the point where the constant of the linear coupling between the two cores is equal to the Bragg-reflectivity coefficient accounting for the linear conversion between the right- and left-traveling waves in each core, i.e., the ES's are the "most endemic" solitary solitons in this system. The stability region quickly shrinks with the increase of the soliton's velocity c, and completely disappears when c exceeds half the maximum velocity. Collisions between stable moving solitons of various types are also considered, with a conclusion that the collisions are always quasielastic.

DOI: 10.1103/PhysRevE.69.066610 PACS number(s): 42.81.Dp, 42.50.Md, 42.65.Tg, 05.45.Yv

I. INTRODUCTION

Light propagation in optical media with a periodic modulation of the refractive index has been a subject of intensive theoretical and experimental studies. Waveguides of this type are used in various applications, which include optical filters, dispersion compensators, switches, pulse compressors, etc. They are also media of fundamental interest in their own right. Applied and fundamental aspects of optics of the periodically modulated waveguides, which are most essential for the present work, were investigated, in particular, in Refs. [1–12] (see also Ref. [13]).

Bragg grating (BG) is a periodic structure which induces linear resonant coupling between counterpropagating waves. The interplay of the counterpropagation and linear coupling gives rise to strong effective dispersion with a gap in the linear spectrum. The balance between the effective dispersion and nonlinearity of the waveguide which carries BG's gives rise to solitary waves, known as gap solitons (GS's) [13–15]. For the first time, they were observed in a 6-cm-long piece of a nonlinear optical fiber equipped with BG's [16].

An optical medium which offers a potential for enhancement of functionality of the nonlinear pulse dynamics is composed of two identical linearly coupled waveguides with the Kerr nonlinearity and resonant gratings in both of them, i.e., a hybrid of the well-known nonlinear optical coupler [17,18] and BG's. As we demonstrate in this work, there is also a physically different realization of the same model, viz., a system of two parallel nonlinear planar waveguides equipped with spatial gratings in the form of a set of parallel scratches. In the latter case, the model describes the dynamics in the spatial, rather than temporal, domain. In particular, the results demonstrated below for collisions between solitons may find a potential application in switching of optical beams (see the Conclusion).

The model of two linearly coupled gratings, which supports GS's, were studied in Ref. [19]. In that work, the existence of asymmetric GS solutions in the bandgap, alongside obvious symmetric solutions, was demonstrated for the case when the linear coupling between the two cores was relatively weak. The asymmetric GS's were stable, while their coexisting symmetric counterparts were unstable. Nevertheless, the symmetric solitons were stable when asymmetric ones did not exist. Recently, a more general model of three linearly coupled fiber gratings forming a triangular configuration was introduced, and various types of symmetric, antisymmetric, and asymmetric solitons were studied [20].

Concerning the realization of these configurations in photonic devices, fabrication of a dual-core fiber grating was reported recently [21]. In fact, the most promising setting for the development of multicore gratings is not a system of parallel-coupled fibers, but rather a photonic-crystal fiber, i.e., a large-area waveguide with many small holes running parallel to its axis [22]. In this host medium, one can easily drill a relatively wide (with the diameter $\sim 2\ \mu$m) hollow conduit (creation of two such conduits in a photonic-crystal fiber was recently reported [23]) and, as was proposed in Ref. [20], one can write an inverted grating on the inner surface of the conduit(s).

The objective of the present work is to extend the study of solitons in the model of the dual-core BG to the case when the linear coupling is stronger, and especially to a region where the intrinsic soliton's frequency may reside inside the continuous spectrum of the radiation modes. Localized solutions whose frequencies are embedded into the continuous

radiation band are usually called embedded solitons (ES's) [24]. ES's have been found in models of various nonlinear-wave systems—chiefly, optical [25–29] and hydrodynamic [30–36]. In contrast with regular solitons, ES's usually do not exist in continuous families, but as isolated solutions, although exceptions to this are known [37], including the physically important case of the nonlinear Schrödinger equation with the third-order dispersion [38], and the complex modified Korteweg–de Vries equation [39].

In this work, we show that continuous families of symmetric and antisymmetric solitons that may be regarded as ES's exist in the model of two linearly coupled BG's with the Kerr nonlinearity. These solutions can be easily found in an exact analytical form, which contains two free parameters, viz., the amplitude of the soliton and its velocity. Moreover, this family exists even in the case when the system's linear spectrum contains no gap at all, hence the model cannot support ordinary GS's. Systematic numerical analysis demonstrates that embedded asymmetric solitons, unlike the abovementioned regular (nonembedded) asymmetric GS's, do not exist in the present model. In other words, this means that only ES's that can be found in the exact analytical form are possible in the model.

Although the fact that the dual-core BG model gives rise to the two-parametric families of symmetric and antisymmetric solitons was not mentioned in any earlier work, the existence of these families is, in fact, obvious. A nontrivial issue is the stability of these solitons, which is the main subject of the present paper. We identify stability regions for both quiescent (zero-velocity) and moving symmetric ES's. In fact, we produce a full stability diagram, that shows stability areas for both regular (nonembedded) and embedded solitons, as a full stability area for regular GS's was not obtained in Ref. [19]. A noteworthy feature is that the stability region of the symmetric ES's extends to the abovementioned case when the system's spectrum has no gap. Concerning the antisymmetric ES's, they all turn out to be unstable, for which a simple explanation, based on consideration of the model's Hamiltonian, is proposed.

In addition to the stability, we also study collisions between solitons of both embedded and ordinary types, which is another natural issue, once stable moving solitons have been found. Simulations of collisions were carried out systematically in the entire region in the parametric space where the stable ES's exist. A general conclusion is that the solitons are stable against collisions, and in all the cases the collisions are quasielastic, giving rise to very small radiation loss. Thus, the colliding solitons either pass through each other, or bounce.

The rest of the paper is organized as follows. In Sec. II, we formulate the model, give its two different physical realizations (in the temporal and spatial domains), and produce analytical solutions for the ES's. Results of the stability analysis are collected in Sec. III, and collisions between moving solitons are considered in Sec. IV. Section V concludes the paper.

II. THE MODEL AND EXACT SOLUTIONS FOR SYMMETRIC SOLITONS

A dual-core nonlinear fiber grating is described by a set of four equations [19]

$$iu_{1t} + iu_{1x} + (|u_1|^2/2 + |v_1|^2)u_1 + v_1 + \lambda u_2 = 0, \tag{1}$$

$$iv_{1t} - iv_{1x} + (|v_1|^2/2 + |u_1|^2)v_1 + u_1 + \lambda v_2 = 0, \tag{2}$$

$$iu_{2t} + iu_{2x} + (|u_2|^2/2 + |v_2|^2)u_2 + v_2 + \lambda u_1 = 0, \tag{3}$$

$$iv_{2t} - iv_{2x} + (|v_2|^2/2 + |u_2|^2)v_2 + u_2 + \lambda v_1 = 0, \tag{4}$$

where t and x are the normalized time and propagation distance, the subscripts 1 and 2 are numbers of the two cores, and the fields denoted by u and v are amplitudes of the right- and left-traveling waves in each core. Alternatively, the same model may be realized as describing stationary field distributions in two parallel-coupled planar waveguides with the gratings in the form of a system of parallel scratches, in which cases t and x are, respectively, the propagation distance and transverse coordinate. In either case, the cross-phase-modulation coefficient and Bragg reflectivity are normalized to be 1, and λ is the coefficient of the linear coupling between the cores. In what follows, we set $\lambda > 0$, as the opposite case reduces to it by taking $-u_2$ and $-v_2$ instead of u_2 and v_2.

The existence of nontrivial soliton states in this model assumes that the Bragg-reflection length in each core should be of the same order of magnitude as the coupling length due to the interaction between the cores. In the fiber gratings available in the experiment, both lengths have typical values between 1 mm and 1 cm [13]; essentially the same estimates apply to the abovementioned alternative realization of the present model, in terms of spatial fields in two parallel planar waveguides with the quasi-one-dimensional gratings. Thus, experimental observation of the solitons studied in Ref. [19] and in the present work is quite feasible (as for the necessary length of the dual-core fiber grating, several centimeters is sufficient [16], and, actually, essentially longer uniform BG's are available [13]). It may also be relevant to mention that, thus far, solitons in the usual nonlinear fiber couplers have not been observed, despite a large amount of theoretical work done for them (see a review in Chap. 6 of Ref. [40]). The addition of the BG offers a realistic possibility to observe solitons in couplers (especially, using the abovementioned configuration with two hollow conduits in a photonic-crystal fiber with inverted BG's written on the inner surfaces).

The linear version of Eqs. (1)–(4) gives rise to a dispersion relation $\omega(k)$ for the plane-wave solutions $u_{1,2}, v_{1,2} \sim \exp(ikx - i\omega t)$. The dispersion relation contains two branches

$$\omega^2 = \lambda^2 + 1 + k^2 \pm 2\lambda\sqrt{1 + k^2}, \tag{5}$$

each having its own gap. The ones corresponding to the upper and lower signs in Eq. (5) are, respectively,

$$|\omega| \leqslant 1 + \lambda, \tag{6}$$

$$|\omega| \leqslant \max\{0, (1 - \lambda)\}. \tag{7}$$

As is seen, the inner gap (7) exists provided that $\lambda < 1$. It is located completely inside the outer one (6), thus the true

bandgap of the full four-wave system is given by the expression (7), provided that $\lambda<1$, and it does not exist if $\lambda\geqslant 1$ [19]. However, the partial bandgap (semi gap) (6) exists at any λ, which opens the way to the possibility of the existence of ES's [24,27–29].

Steady-state solutions to Eqs. (1)–(4) for solitons moving at a velocity c are sought for as

$$u_{1,2}(\xi,t)=e^{-i\omega t}U_{1,2}(\xi),v_{1,2}(\xi,t)=e^{-i\omega t}V_{1,2}(\xi),\xi\equiv x-ct. \tag{8}$$

Substitution of Eqs. (8) into Eqs. (1)–(4) leads to a set of four ODE's,

$$\omega U_1+i(1-c)U_1'+(|U_1|^2/2+|V_1|^2)U_1+V_1+\lambda U_2=0, \tag{9}$$

$$\omega V_1-i(1+c)V_1'+(|V_1|^2/2+|U_1|^2)V_1+U_1+\lambda V_2=0, \tag{10}$$

$$\omega U_2+i(1-c)U_2'+(|U_2|^2/2+|V_2|^2)U_2+V_2+\lambda U_1=0, \tag{11}$$

$$\omega V_2-i(1+c)V_2'+(|V_2|^2/2+|U_2|^2)V_2+U_2+\lambda V_1=0, \tag{12}$$

where the prime stands for $d/d\xi$. To find symmetric or asymmetric soliton solutions, numerical and approximate analytical (based on the variational technique) methods can be used, as was done in Ref. [19], where both moving ($c\neq 0$) and quiescent ($c=0$) asymmetric and symmetric stable solitons of the usual (nonembedded) type were found. However, an actual stability border for asymmetric solitons was not found in Ref. [19], as the analysis was limited to the case of a small coupling constant λ. This result is presented in Fig. 1 below. Parametric regions which were not investigated before are explored below to search for new stable soliton solutions, especially ES ones.

Solutions for symmetric solitons, with

$$u_1=u_2,v_1=v_2, \tag{13}$$

can be easily obtained in an exact form, using well-known solutions for the single-core model [41,42]. In the case of $c=0$, the result is

$$u_{1,2}(\xi,t)=e^{-i(\chi-\lambda)t}U(\xi),v_{1,2}(\xi,t)=-e^{-i(\chi-\lambda)t}U^*(\xi) \tag{14}$$

(the asterisk stands for the complex conjugation), where the function $U(\xi)$ obeys the equation

$$\chi U+iU'+(3/2)|U|^2U-U^*=0. \tag{15}$$

A family of exact solutions to Eq. (15) is well known,

$$U(x)=\sqrt{\frac{2}{3}}(\sin\theta)\,\mathrm{sech}\left(x\sin\theta-\frac{i}{2}\theta\right),V=-U^*, \tag{16}$$

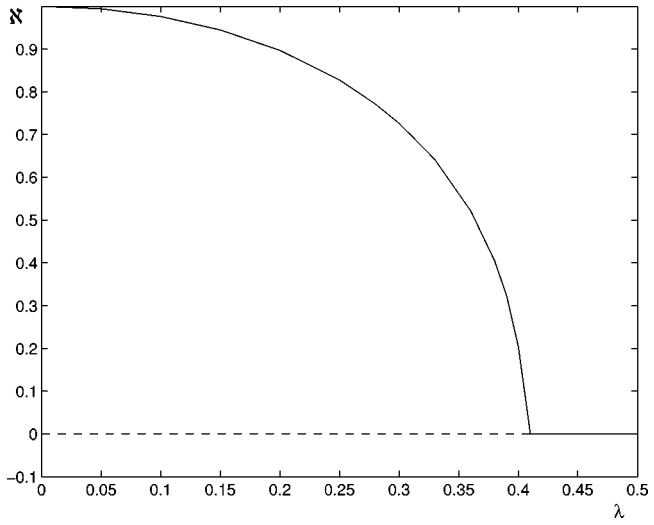

FIG. 1. The bifurcation diagram for stationary gap solitons with $\theta=0.4\pi$. The curved branch corresponds to the asymmetric soliton solutions, while the horizontal line represents the symmetric solutions. Stable and unstable branches are shown by solid and dashed lines, respectively. Note that the asymmetric solutions exist only inside the true bandgap: a condition for this, following from Eqs. (7) and (18), is $2\lambda<1+\cos(0.4\pi)\approx 1.309$, and it is obvious that this condition is met.

$$\theta\equiv\cos^{-1}\chi, \tag{17}$$

where θ is an intrinsic parameter of the soliton family, which is proportional to the soliton energy and takes values $0<\theta<\pi$.

A simple but important remark is that, as the exact solutions (16) and (17) to Eq. (15) exist in the interval $-1<\chi<+1$, the frequency of the solitons corresponding to the expressions (14) falls into an interval

$$-1-\lambda<\omega_{\mathrm{symm}}\equiv\chi-\lambda<1-\lambda, \tag{18}$$

which is, obviously, *broader* than the bandgap (7), although it is always located inside the semigap (6). This means that, in the case of $\lambda<1$, the exact symmetric solitons belonging to the subinterval

$$-1-\lambda<\omega_{\mathrm{symm}}<-|1-\lambda| \tag{19}$$

may be classified as embedded solitons (ES's). Moreover, in the case of $\lambda>1$, when the true bandgap (7) of the four-wave system does not exist at all, the exact symmetric solutions are still available in the interval (18).

On the other hand, the substitution (13), as well as the similar substitution (25) for the antisymmetric case, condenses the underlying system of four equations (1)–(4) into a system of two equations equivalent to the usual [15] single-core fiber-grating model. In terms of the reduced model, the symmetric and antisymmetric solitons are regular GS's, rather than ES's (this may be compared to the situation for solitons in the usual two-core fiber, without the BG [43]). Nevertheless, small perturbations added to the soliton may violate the reduction (13) and (25), and they thus "feel" the actual band structure of the full four-wave system. Therefore,

stability of the symmetric and antisymmetric solitons in the four-wave system may be completely different from that of the regular two-wave GS's (which is the case indeed, as shown below), revealing the "hidden embeddedness" of the symmetric and antisymmetric solitons.

Symmetric moving solitons (with $c \neq 0$) are looked for in the form

$$u_{1,2}(x,t) \equiv u(x,t) = e^{i\lambda t}\overline{u}(x,t); v_{1,2}(x,t) \equiv v(x,t) = e^{i\lambda t}\overline{v}(x,t). \tag{20}$$

The substitution of these expressions into Eqs. (1)–(4) results in a system

$$i\overline{u}_t + i\overline{u}_x + (|\overline{u}|^2/2 + |\overline{v}|^2)\overline{u} + \overline{v} = 0, \tag{21}$$

$$i\overline{v}_t - i\overline{v}_x + (|\overline{v}|^2/2 + |\overline{u}|^2)\overline{v} + \overline{u} = 0. \tag{22}$$

Moving-soliton solutions to Eqs. (21) and (22) are well known [41,42]:

$$\overline{u} = \alpha W(X)\exp\,[y/2 + i\phi(X) - iT\cos\,\theta + i\phi_0],$$

$$\overline{v} = -\alpha W^*(X)\exp\,[-y/2 + i\phi(X) - iT\cos\,\theta + i\phi_0], \tag{23}$$

where ϕ_0 is an arbitrary real constant and

$$\alpha^{-2} \equiv \frac{3}{2} + c^2, \tanh y \equiv c, X \equiv \frac{x - ct}{\sqrt{1-c^2}}, T \equiv \frac{t - cx}{\sqrt{1-c^2}},$$

$$\phi(X) = \alpha^2\,\sinh(2y)\tan^{-1}[\tanh\,(X\,\sin\theta)\tan(\theta/2)],$$

$$W(X) = (\sin\,\theta)\,\mathrm{sech}\,[X\,\sin\,\theta - i(\theta/2)]. \tag{24}$$

Solutions for antisymmetric solitons with

$$u_1 = -u_2, v_1 = -v_2 \tag{25}$$

can also be easily found in an exact form. For zero-velocity antisymmetric solitons, Eq. (14) is replaced by

$$u_1(\xi,t) = e^{-i(\chi+\lambda)t}U(\xi), v_1(\xi,t) = -e^{-i(\chi+\lambda)t}U^*(\xi), \tag{26}$$

where $U(\xi)$ again obeys Eq. (15) and is thus given by the expressions (16) and (17). So, Eqs. (26) imply that the antisymmetric soliton solutions exist in the interval

$$-1 + \lambda < \omega_{\mathrm{anti}} \equiv \chi + \lambda < 1 + \lambda, \tag{27}$$

which is again broader than the true bandgap (7) but smaller than the semigap (6), see Eq. (18). In particular, they occupy a subinterval [see Eq. (19)]

$$|1 - \lambda| < \omega_{\mathrm{anti}} < 1 + \lambda, \tag{28}$$

where they are ES's, as it does not overlap with the true bandgap (7), and they exist also in the case of $\lambda > 1$, when the four-wave system has no true bandgap.

Solutions for antisymmetric moving solitons are looked for, instead of Eq. (20), in the form

$$u_1(x,t) \equiv u(x,t) = e^{-i\lambda t}\overline{u}(x,t); v_1(x,t) \equiv v(x,t) = e^{-i\lambda t}\overline{v}(x,t). \tag{29}$$

Again, the functions $\overline{u}$ and $\overline{v}$ obey Eqs. (21) and (22), and are given by the expressions (23).

III. STATIONARY SOLITONS AND THEIR STABILITY

A. Regular (nonembedded) asymmetric solitons

Symmetric and asymmetric soliton solutions for the present model, found in Ref. [19] for the case of small coupling constant, are presented by dint of a bifurcation diagram in Fig. 1, which is a plot of the asymmetry parameter

$$\aleph \equiv \frac{u_{1m}^2 - u_{2m}^2}{u_{1m}^2 + u_{2m}^2} \tag{30}$$

versus the coupling constant λ, u_{1m} and u_{2m} being the amplitudes of the fields $u_{1,2}$ in the two cores. The diagram demonstrates the appearance of stable asymmetric solutions and simultaneous destabilization of the symmetric one at a critical value of λ. Due to symmetries of Eqs. (9)–(12), the bifurcation diagram for $\lambda < 0$ is the mirror image of that with $\lambda > 0$. In fact, this diagram was already obtained in Ref. [19], and is included here for completeness of the description.

However, existence and stability limits for the solitons were found in Ref. [19] only in a partial form, therefore the global picture of stable and unstable soliton solutions remained unexplored (it was displayed in a more complete form for the abovementioned system of *three* linearly coupled fiber gratings, forming a triangular configuration, in the recent work [20]). The first result of the present work is a full stability diagram for the quiescent (zero-velocity) solitons, both GS's and ES's, in the model based on Eqs. (1)–(4), which is displayed in Fig. 2 in terms of the (λ, θ) plane [recall θ is the intrinsic parameter of the soliton solution defined by Eq. (17)]. The stability and instability was identified in direct simulations, which is not as rigorous as the definition based on computation of stability eigenvalues for small perturbations [44], but it is closer to the stability as it may be observed in the experiment. In particular, a noteworthy peculiarity, obvious in Fig. 2, is that stable symmetric ES never (at no value of λ) coexist with stable asymmetric GS's, while their coexistence with stable symmetric regular GS's occurs.

The area above $\theta = 0.5\pi$ is not included, as all solitons are unstable if θ exceeds a critical value $\approx 1.01(\pi/2)$ [44,45]. We note in passing that the instability of solitons in that area can be effectively controlled in a model including a local attractive defect [46,47]: the unstable solitons quickly relax to a stable one with $\theta \approx 0.5\pi$ by shedding off excess energy in the form of radiation.

B. Quiescent (zero-velocity) embedded solitons

Any soliton which exists below the bandgap edge in Fig. 2 is classified as an ES, in the sense that was explained above. Such solitons were not considered in the present model before. Here, we started by seeking for ES's, different

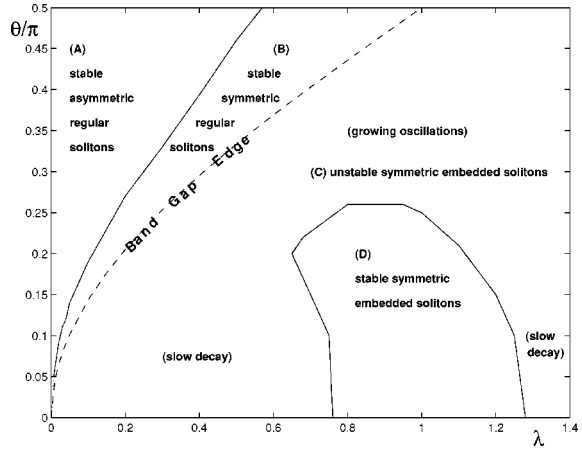

FIG. 2. Regions in the (λ, θ) plane, where different types of standing ($c=0$) gap solitons are found [recall that θ is the intrinsic parameter of the soliton family, see Eq. (16)]. In region A, stable asymmetric regular (nonembedded) solitons exist in the bandgap (note that it ends at $\lambda=1$, in accordance with Eq. (7). In region B, symmetric regular solitons are stable. The bandgap edge is identified as a curve where the frequency of the exact soliton, given by Eqs. (14) and (16), is equal to $1-\lambda$, which is the edge of the gap in the linear spectrum of the four-wave system (2)–(4), see Eq. (7) (in particular, for $\lambda=1$, the bandgap edge is at $\theta=\pi/2$). Below the bandgap edge, only solitons of the embedded type (in terms of the full four-wave system) may exist. They are unstable in region C, but *stable* in region D, where λ is close to 1, and θ is small. Note that the latter stability region extends to values $\lambda>1$, where the system has no true bandgap gap in its spectrum.

from the exact solutions given above, in a numerical form. The systematic search in the system's parameter space had turned up *no* new (asymmetric) ES solutions, which is a drastic difference from the situation inside the bandgap, where the obvious exact symmetric and antisymmetric solitons coexist with nontrivial asymmetric ones [19]. Note that the region occupied by asymmetric solitons in Fig. 2 is isolated from the bandgap's edge.

Nevertheless, the exact symmetric solitons, given by the expressions (13), (14), (16), and (17), and their antisymmetric counterparts, given by Eqs. (25), (26), (16), and (17), exist as a continuous family of the ES's in the interval (19), if $\lambda<1$, and in the whole interval (18) if $\lambda>1$, or in the intervals (28) and (27), respectively. A nontrivial issue is their stability. Indeed, as was shown in a general form in Ref. [24], ES's are linearly but nonlinearly semi stable (which means that, beyond the linear approximation, a weak instability may be initiated by a small perturbation, depending on its sign), in the case when they exist as isolated solutions. In actual simulations, the semistable ES's may behave, in some parameter regions, as truly stable solitons [28,29]. In the case when ES's can be found in continuous families, they are, generally speaking, semistable too [38].

In this work, we focus on investigation of the stability of the continuous-family ES's, running direct simulations in a systematic way, with random perturbations added to the soliton wave form. As was mentioned above, this approach is adequate to predict a possibility of observation of ES's in an experiment. This way, the existence interval of the ES's was

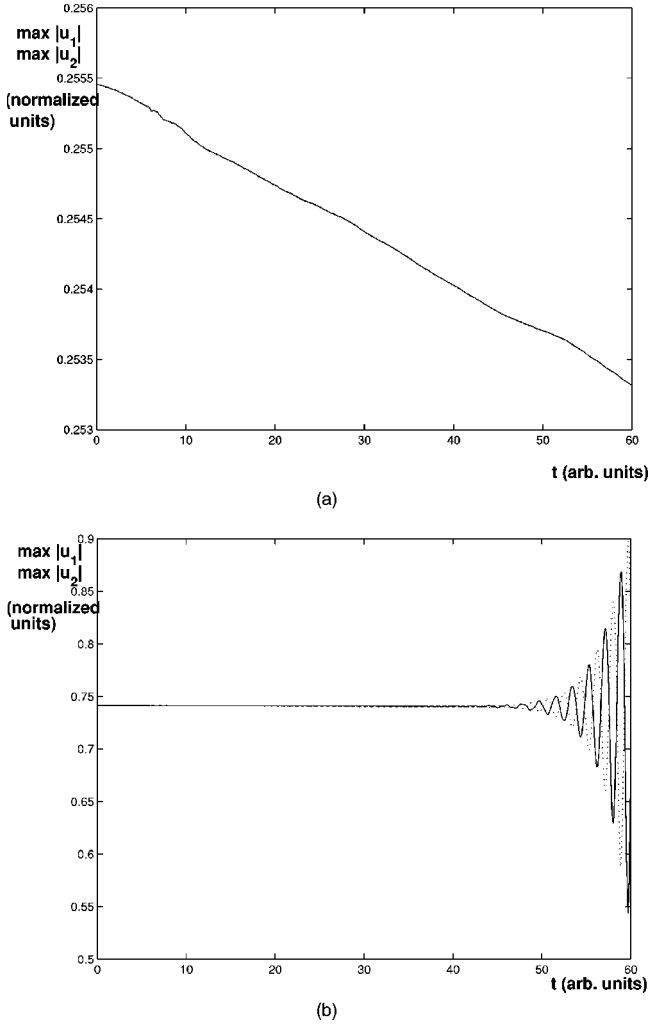

FIG. 3. Typical examples of the evolution of unstable symmetric embedded solitons. The time dependence of the amplitudes of the soliton, i.e., maxima of $|u_1|$ (solid) and $|u_2|$ (dotted), is displayed. The decay of the fields v_1 and v_2 is similar. (a) $c=0$, $\lambda=0.7$, and $\theta=0.1\pi$ (in this case, the solid and dotted lines completely overlap). (b) $c=0$, $\lambda=0.7$, and $\theta=0.3\pi$, which is larger than in panel (a).

scanned for their stability. The numerical method was based on the split-step code combined with the Fourier transform.

We stress that not all the symmetric ES's, available in the exact analytical form, are stable. Their stability region has a nontrivial shape, and it is included in the general stability diagram displayed in Fig. 2. It can be seen that the stable symmetric solitons cluster around the region with small θ and $\lambda\approx1$, where the bandgap (7) closes up. Outside this region, the symmetric ES's are unstable; however, the instability is weak, and develops slowly near borders of the stability region.

The simulations demonstrate that unstable symmetric ES's with a small amplitude $\theta\simeq0.1\pi$, decay into radiation. See an example in Fig. 3(a); in this case, the solitons decay and remain symmetric, i.e., without violating the reduction (13) which lead to the exact symmetric solutions. Unstable solitons with a larger amplitude $\theta\gtrsim0.3\pi$ first develop oscillations [see Fig. 3(b)], but eventually they also decay. It is seen from Fig. 3(b) that, in the latter case, the perturbations

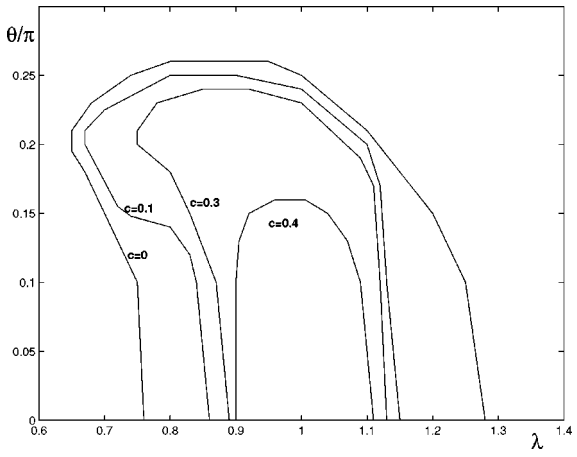

FIG. 4. Regions in the (λ, θ) plane, where the moving symmetric embedded solitons are stable. With the increase of the velocity $|c|$, the stability region shrinks to nil at $c \approx 0.5$.

which destroy the stable ES are antisymmetric, i.e., they violate the reduction (13) and arouse full dynamics of the four-wave system.

The antisymmetric quiescent solitons are *always* unstable, both outside the true bandgap and inside of it. All of them decay, although the ones with λ close to 1 and small θ do it slower than those with λ taken farther away from 1. Unstable antisymmetric solitons with $\theta \gtrsim 0.3\pi$ develop oscillations similar to those demonstrated by their unstable symmetric counterparts.

In fact, the instability of the antisymmetric solitons has a simple explanation: a part of the Hamiltonian H of the underlying model (1) and (2), which accounts for the linear coupling between the cores, is

$$H_{\text{coupling}} = -\lambda \int_{-\infty}^{+\infty} (u_1^* u_2 + v_1^* v_2) dx + \text{c.c.},$$

where c.c. stands for the complex-conjugate expression. As it immediately follows from here, the substitutions (13) and (25) yield, respectively, $H_{\text{coupling}} < 0$ and $H_{\text{coupling}} > 0$ (recall we set $\lambda > 0$), while making no difference in other parts of the full H. Obviously, a symmetric state which minimizes H may give rise to a stable solution, but an antisymmetric one, which corresponds to the maximum of H, cannot do it.

C. Moving embedded solitons

The stability of moving symmetric ES's, which are available in the exact analytical form, given by Eqs. (13), (20), (23), and (24), was also examined in direct simulations. The evolution of the stability region in the plane (λ, θ) with the increase of the velocity $|c|$ is shown in Fig. 4. It is seen that the stability region quickly shrinks with the increase of the velocity c, and no stable moving symmetric ES's can be found for $c \gtrsim 0.5$. This is a drastic difference from what is known about stability of the moving regular GS's in the standard single-core model, where the critical value of θ separating stable and unstable solitons very little depends on the velocity, in the whole region $0 \leqslant c < 1$ [44].

Similar to what was found for quiescent symmetric solitons, the instability of the moving ones develops slowly close to the border of the stability region. The unstable moving solitons with small θ decay into radiation in a way similar to what is depicted in Fig. 3(a). "Heavier" moving solitons (the ones with larger θ) develop oscillations similar to those in Fig. 3(b), although the oscillations start to develop at smaller θ (close to $\theta = 0.2\pi$) than in the quiescent solitons. The latter feature seems quite natural, in view of the shrinkage of the stability region with the increase of the velocity, as per Fig. 4.

IV. COLLISIONS BETWEEN SOLITONS

Stable moving ES's being available, it is natural to consider their collisions, with regular solitons (stable GS's inside the bandgap), or between ES's themselves. We display the results here for a fixed value of the linear-coupling coefficient $\lambda = 0.9$. As it is smaller than 1, regular GS's exist in this case too. In fact, we carried out simulations at other values of λ too—in particular, in the range $0.7 < \lambda < 1$. The results are consistent with what is described below. However, when λ is close to 0.7 or to 1, either the symmetric ES's or the regular GS's are too close to the instability threshold, therefore the case with $\lambda = 0.9$ is more interesting, corresponding to collisions between sufficiently robust solitons. Only collisions between symmetric solitons were considered, since asymmetric GS's do not coexist with any stable ES for the same value of λ, according to Fig. 2.

Figure 5(a) shows an example of a moving ES colliding with a quiescent ES, the two solitons being in phase at the initial moment. It is seen that the solitons repel each other and essentially bounce from each other as particles, so that the initially moving soliton stops, while the initially quiescent one picks up all the momentum. Very little radiation loss is observed, so that the collision is almost entirely elastic. The same collision with different values of the initial phases (including the π-out-of-phase case) seems virtually the same way: the former quiescent soliton starts to run, while the former moving one halts. In this connection, it should be said that, in the case when the colliding solitons have different amplitudes and/or absolute values of the velocities, i.e., if the collision is not a fully symmetric one, the initial phase difference between the solitons is not expected to play an essential role.

Figure 5(b) shows the collision of a moving ES with a quiescent regular GS, both being initially in phase. This time, the moving soliton *passes* through the quiescent one, with small radiation loss. The quiescent soliton gets shifted as a result of the collision. Essentially the same result takes place for other values of the initial phase difference between the solitons.

Figure 5(c) shows the cases when both colliding solitons are of the embedded type, and both are moving (but with different velocities). This case is not equivalent to that considered above in Fig. 5(a), as the underlying equations (1)–(4) are not Galilean or Lorentz invariant, hence no velocity change can be generated by a simple transformation. The outcome of the collision is also very different from that

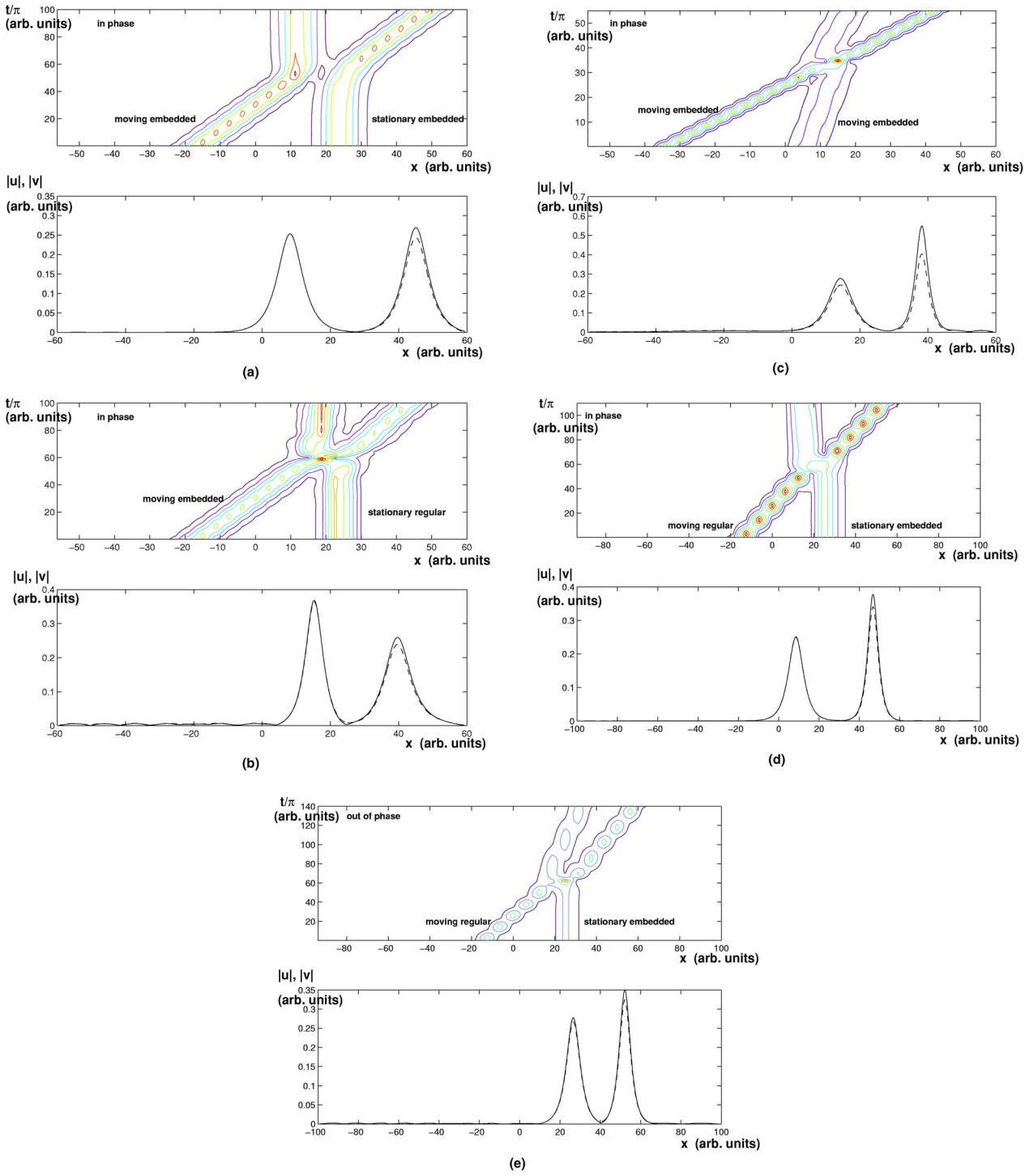

FIG. 5. Typical examples of collisions between symmetric solitons. The intercore linear coupling coefficient λ is fixed to be 0.9. The upper panels show the contour plots of the evolution of $|u_1|$, and the lower ones display the wave forms of $|u_1|$ and $|v_1|$ (solid and dashed lines) at the end of the simulation. (a) A moving embedded soliton with $c=0.1$ and $\theta=0.1\pi$ collides with a quiescent ($c=0$) embedded soliton, which also has $\theta=0.1\pi$. Both solitons are initially in phase. (b) A moving embedded soliton with $c=0.1$ and $\theta=0.1\pi$ collides with a quiescent ($c=0$) regular one with $\theta=0.5\pi$, both solitons being initially in phase. The moving embedded soliton passes through the quiescent regular gap soliton, which undergoes a position shift. Small radiation loss occurs in this case. (c) A moving embedded soliton with $c=0.3$ and $\theta=0.2\pi$ collides with another moving embedded soliton that has $c=0.1$ and $\theta=0.1\pi$, both solitons being initially in phase. The heavier fast soliton passes through the slow lighter one, which undergoes a position shift. The collision results in small radiation loss. (d) A moving regular soliton with $c=0.1$ and $\theta=0.5\pi$ collides with a quiescent ($c=0$) embedded one with $\theta=0.1\pi$. Initially, both solitons are in phase. (e) The same as in the case (d), but with the initial phase difference π between the solitons. Note that, in contrast with the case (d), both solitons move after the collision.

in Fig. 5(a): this time, the fast soliton passes through the slow one with a very small radiation loss. The slow soliton demonstrates a position shift after the collision. This outcome is actually similar to that observed in Fig. 5(b), despite the fact that the quiescent soliton was a regular one in that case.

Figures 5(d) and 5(e) show the situation when moving regular solitons collide with initially quiescent ES's. In these cases, the heavy moving solitons pass through the lighter quiescent ones. In the case (d), the quiescent soliton demonstrates a position shift. However, the case (e) [which differs from (d) only by the initial phase difference between the solitons, which is π, rather than 0], is remarkably different: in this case, the former quiescent solitons also acquires a *finite velocity* after the collision. In all these cases, very small radiation loss results from the collisions.

The case when both colliding solitons are regular ones was studied too. The collisions then seem essentially the same way as in the case when the ES's collide, see Fig. 5(a).

If the model is realized in terms of the spatial solitons in planar waveguides (see the Introduction), the shift of the soliton and (in some cases) its velocity change, which result from the collision, can find application to switching of the beams. In that case, the soliton which features the position shift or velocity change (in the spatial-domain case, the latter actually is a change of the beam's slant) may be a signal beam, while the other one is a control one.

V. CONCLUSION

In this work, we have demonstrated that the four-wave model, describing two linearly coupled symmetric nonlinear waveguiding cores with the Bragg grating written on each of them, supports a two-parametric family of exact symmetric and antisymmetric solitons, whose existence domains cover the system's bandgap and extend into the "semigap" (which is a gap only in terms of one out of two branches of the dispersion relation). Therefore, parts of these solution families may be regarded as embedded solitons. The model itself has two different physical realizations, for fibers and planar waveguides—in the temporal and spatial domains, respectively. The embedded-soliton family is found even in the case when the system's spectrum has no true bandgap at all, hence no regular gap solitons may exist. Numerical search has revealed that the system never supports asymmetric embedded solitons.

Simulations of the evolution of perturbed solitons have produced a full stability diagram, which comprises both embedded and regular (gap) solitons and quiescent and moving ones. The stability region of the embedded solitons is located around the point where the two linear couplings (the intercore and Bragg-reflectivity ones) are equal. The latter finding implies that the embedded solitons are most "endemic" to this system. Their stability region shrinks with the increase of the soliton velocity c, so that there are no stable embedded solitons for the velocity exceeding half of the maximum velocity. All the antisymmetric embedded solitons, quiescent and moving ones, are unstable, to which a simple explanation is given, based on the consideration of the system's Hamiltonian. Collisions between solitons of different types have been studied too, with the conclusion that the collisions always result in the mutual passage or bounce of the solitons, with very small radiation energy losses.

ACKNOWLEDGMENTS

One of the authors (B.A.M.) appreciates the hospitality of the Optoelectronic Research Centre at the Department of Electronic Engineering, City University of Hong Kong. He is also indebted to J. Yang for making Ref. [38] available prior to publication.

[1] C. M. Ragdale, D. Reid, and I. Bennion, Proc. SPIE **1171**, 148 (1989).
[2] F. Ouellette, Opt. Lett. **12**, 847 (1987).
[3] P. A. Krug, T. Stephens, G. Dhosi, G. Yoffe, F. Ouellette, and P. Hill, Electron. Lett. **31**, 1091 (1995).
[4] R. I. Laming, N. Robinson, A. Cavaciuti, F. Vaninetti, C. J. Anderson, M. N. Zervas, and M. J. Cole, IEEE Photonics Technol. Lett. **8**, 944 (1996).
[5] N. M. Litchinitser, B. J. Eggleton, and D. B. Patterson, J. Lightwave Technol. **15**, 1303 (1997).
[6] B. J. Eggleton, T. Stephens, P. A. Krug, G. Dhosi, Z. Brodzeli, and F. Ouellette (unpublished).
[7] S. Radic, N. George, and G. P. Agrawal, J. Opt. Soc. Am. B **12**, 671 (1995).
[8] H. G. Winful, J. H. Marburger, and E. Garmire, Appl. Phys. Lett. **35**, 379 (1979).
[9] N. D. Sankey, D. F. Prelewitz, and T. G. Brown, Appl. Phys. Lett. **60**, 1427 (1992).
[10] M. Cada, J. He, B. Acklin, M. Proctor, D. Martin, F. Morier-Genoud, M. A. Dupertuus, and J. M. Glinsky, Appl. Phys. Lett. **60**, 404 (1992).
[11] C. J. Herbert and M. S. Malcuit, Opt. Lett. **18**, 1783 (1993).
[12] H. G. Winful, Appl. Phys. Lett. **46**, 527 (1985).
[13] R. Kashyap, *Fiber Bragg Gratings* (Academic Press, San Diego, 1999).
[14] G. P. Agrawal, *Nonlinear Fiber Optics* (Academic Press, San Diego, 1989).
[15] C. M. de Sterke and J. E. Sipe, Prog. Opt. **33**, 203 (1994).
[16] B. J. Eggleton, R. E. Slusher, C. M. de Sterke, P. A. Krug, and J. E. Sipe, Phys. Rev. Lett. **76**, 1627 (1996).
[17] S. M. Jensen, IEEE J. Quantum Electron. **QE-18**, 1580 (1982).
[18] A. M. Maier, Kvantovaya Elektron. (Moscow) **9**, 2996 (1982).
[19] W. C. K. Mak, B. A. Malomed, and P. L. Chu, J. Opt. Soc. Am. B **15**, 1685 (1998).
[20] A. Gubeskys and B. A. Malomed, Eur. Phys. J. D **28**, 283 (2004).
[21] M. Åslund, L. Poladian, J. Canning, and C. M. de Sterke, J. Lightwave Technol. **20**, 1585 (2002).
[22] T. M. Monro and D. J. Richardson, C. R. Phys. **4**, 175 (2003).

[23] W. N. MacPherson, J. D. C. Jones, B. J. Mangan, J. C. Knight, and P. St .J. Russell, Opt. Commun. **223**, 375 (2003).
[24] J. Yang, B. A. Malomed, and D. J. Kaup, Phys. Rev. Lett. **83**, 1958 (1999).
[25] D. J. Kaup, T. I. Lakoba, and B. A. Malomed, J. Opt. Soc. Am. B **14**, 1199 (1997).
[26] P. K. A. Wai, H. H. Chen, and Y. C. Lee, Phys. Rev. A **41**, 426 (1990).
[27] A. R. Champneys and B. A. Malomed, J. Phys. A **32**, L547 (1999).
[28] A. R. Champneys, B. A. Malomed, J. Yang, and D. J. Kaup, Physica D **152-153**, 340 (2001).
[29] J. Yang, B. A. Malomed, D. J. Kaup, and A. R. Champneys, Math. Comput. Simul. **56**, 585 (2001).
[30] Y. Pomeau, A. Ramani, and G. Grammaticos, Physica D **31**, 127 (1988).
[31] V. I. Karpman, Phys. Rev. E **47**, 2073 (1993).
[32] J. P. Boyd, Physica D **48**, 129 (1991).
[33] R. Grimshaw and N. Joshi, SIAM (Soc. Ind. Appl. Math.) J. Appl. Math. **55**, 124 (1995).
[34] T. R. Akylas and T. S. Yang, Stud. Appl. Math. **94**, 1 (1995).
[35] T. S. Yang and T. R. Akylas, Phys. Fluids **8**, 1506 (1996).
[36] T. S. Yang and T. R. Akylas, J. Fluid Mech. **330**, 215 (1997).
[37] J. Yang, Stud. Appl. Math. **106**, 337 (2001).
[38] J. Yang and T. R. Akylas (unpublished).
[39] R. F. Rodríguez, J. A. Reyes, A. Espinosa-Cerón, J. Fujioka, and B. A. Malomed, Phys. Rev. E **68**, 036606 (2003).
[40] B. A. Malomed, Prog. Opt. **43**, 71 (2002).
[41] A. B. Aceves and S. Wabnitz, Phys. Lett. A **141**, 37 (1989).
[42] D. N. Christodoulides and R. I. Joseph, Phys. Rev. Lett. **62**, 1746 (1989).
[43] A. A. Akhmediev and A. Ankiewicz, Phys. Rev. Lett. **70**, 2395 (1993); B. A. Malomed, I. Skinner, P. L. Chu, and G. D. Peng, Phys. Rev. E **53**, 4084 (1996).
[44] I. V. Barashenkov, D. E. Pelinovsky, and E. V. Zemlyanaya, Phys. Rev. Lett. **80**, 5117 (1998).
[45] B. A. Malomed and R. S. Tasgal, Phys. Rev. E **49**, 5787 (1994).
[46] William C. K. Mak, B. A. Malomed, and P. L. Chu, J. Opt. Soc. Am. B **20**, 725 (2003).
[47] William C. K. Mak, B. A. Malomed, and P. L. Chu, Phys. Rev. E **67**, 026608 (2003).